Author Manuscript
Accepted for publication in a peer-reviewed journal

NIST National Institute of Standards and Technology • U.S. Department of Commerce

Published in final edited form as:
Chem Mater. 2020 ; 32(6): .

The Influence of Additives on the Interfacial Width and Line Edge Roughness in Block Copolymer Lithography

Daniel F. Sunday[1,†,*], **Xuanxuan Chen**[2,†], **Thomas R. Albrecht**[3], **Derek Nowak**[3], **Paulina Rincon Delgadillo**[4], **Takahiro Dazai**[5], **Ken Miyagi**[5], **Takaya Maehashi**[5], **Akiyoshi Yamazaki**[5], **Paul F. Nealey**[2], **R. Joseph Kline**[1]

[1]Materials Science and Engineering Division, National Institute of Standards and Technology, 100 Bureau Drive, Gaithersburg, MD 20899

[2]Institute for Molecular Engineering, University of Chicago, 5801 S Ellis Ave, Chicago, IL 60637

[3]Molecular Vista, San Jose, CA 95119, U.S.A

[4]IMEC, Kapeldreef 75, Leuven B-3001, Belgium

[5]Tokyo Ohka Kogyo, 1590 Tabata, Samukawa-Machi, Koza-Gun, Kanagawa 253-0114, Japan

Abstract

The challenges of patterning next generation integrated circuits have driven the semiconductor industry to look outside of traditional lithographic methods in order to continue cost effective size scaling. The directed self-assembly (DSA) of block copolymers (BCPs) is a nanofabrication technique used to reduce the periodicity of patterns prepared with traditional optical methods. BCPs with large interaction parameters (χ_{eff}), provide access to smaller pitches and reduced interface widths. Larger χ_{eff} is also expected to be correlated with reduced line edge roughness (LER), a critical performance parameter in integrated circuits. One approach to increasing χ_{eff} is blending the BCP with a phase selective additive, such as an Ionic liquid (IL). The IL does not impact the etching rates of either phase, and this enables a direct interrogation of whether the change in interface width driven by higher χ_{eff} translates into lower LER. The effect of the IL on the layer thickness and interface width of a BCP are examined, along with the corresponding changes in LER in a DSA patterned sample. The results demonstrate that increased χ_{eff} through additive blending will not necessarily translate to a lower LER, clarifying an important design criterion for future material systems.

Graphical Abstract

*Corresponding author: Daniel.Sunday@nist.gov.
†These authors contributed equally to this work.

Supporting Information
The supporting information is available free of charge at https://pubs.acs.org.
FTIR spectra of [BMPR][TFSI], SLD profiles, additional reflectivity simulations, and the calculated BCP area/junction.

NIST Author Manuscript
NIST Author Manuscript
NIST Author Manuscript

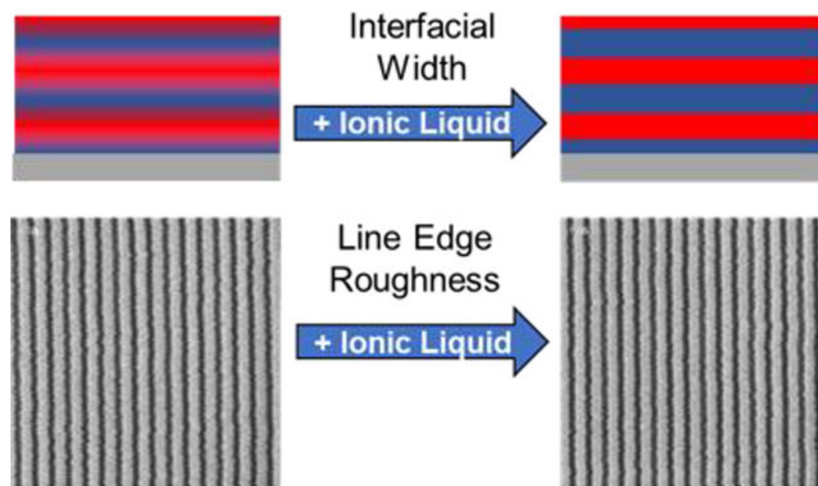

Introduction

The semiconductor industry has relied on advances in lithographic techniques to continue reducing the size of features in integrated circuits. Extreme ultraviolet lithography (EUV) has been projected as the replacement for 193 nm lithography, but technological and economic challenges have delayed its wide scale implementation.[1] As a result the industry has sought alternative solutions for patterning smaller features including multiple patterning steps,[2] nanoimprint[3] and the directed self-assembly (DSA) of block copolymers (BCPs). [4–7] DSA utilizes existing lithographic techniques to pattern a guiding template and the BCP is assembled on the guide, amplifying the pattern density. Polystyrene-*b*-poly(methyl methacrylate) (PS-*b*-PMMA) is the standard material used for DSA due to its ease of assembly and significant progress has been made in developing DSA processes using PS-*b*-PMMA for high volume manufacturing.[8] Unfortunately PS-*b*-PMMA cannot be used to pattern sub-10 nm features due to its small Flory-Huggins interaction parameter (χ_{eff}). As a result, there is a need for materials which can pattern features with even smaller sizes and to resolve outstanding issues such as defect density and line edge roughness (LER).[8–11] The synthetic community has responded to this challenge by developing BCPs with large χ_{eff},[12–22] and as a result there are now numerous demonstrations of DSA with sub-10 nm features.[23–25] Controlling LER is proving to be more complex, as LER originates from a combination of materials properties and processing steps, etching in particular.[26] While it is anticipated that the LER will be proportional to the interface width(w_m), which is in turn proportional to $\chi_{eff}^{-1/2}$, there has yet to be clear evidence that an decrease in w_m is sufficient for a reduction in LER. In addition to developing new BCP chemistries χ_{eff} can be increased by blending BCPs with homopolymers,[27–31] small molecules,[32–35] salts[36–38] or ionic liquids (ILs).[39–41] Using an additive with specific interactions with one of the blocks enables an increase in χ_{eff} without the challenge of developing a new chemistry. To investigate the relationship between χ_{eff} and LER we studied a blend of PS-*b*-PMMA with an ionic liquid, N-butyl-N-methylpyrrolidinium bis(trifluoromethylsulfonyl)imide ([BMPR][TFSI]) (Structures shown in Figure 1). In order to quantify the impact of the IL on PS-*b*-PMMA w_m and L_0 were probed using resonant soft X-ray reflectivity (RSoXR) and infrared

NIST Author Manuscript NIST Author Manuscript NIST Author Manuscript

photoinduced force microscopy (IR-PIFM). The results from this measurement are compared to the LER of a PS-*b*-PMMA/([BMPR][TFSI] blend patterned with DSA.

The DSA of BCPs utilizes a combination of chemo and grapho epitaxy to align a BCP with an underlying pattern and reduce the periodicity. This approach has been successful for the two major integrated circuit features, line-space patterns[4,6,7] and contact holes.[42,43] The guiding pattern is formed with optical techniques such as 193 nm or EUV lithography. In the case of line-space patterns this generally involves etching a guiding stripe into a cross-linked polymer mat which has preferential affinity for one of the blocks, followed by backfilling the pattern with a random copolymer whose composition is tuned to be nearly neutral for both blocks.[44] The BCP is then deposited and in some cases solvent annealing[45,46] or a surface treatment[47,48] is used to promote vertical orientation of the lamellae. After annealing the BCP is then used as an etch mask to transfer the pattern into the underlying substrate. Etching will either rely on the intrinsic etch contrast between the BCP components or can be enhanced using an infiltration synthesis.[49] A variety of BCPs have been developed which have both high χ_{eff} and intrinsic etch contrast, and there have been successful demonstrations of DSA with these materials, reaching periodicities below 10 nm.[22,50] There are also a variety of techniques which are being developed to promote improved kinetics and reduced defects in the self-assembly process, particularly for high χ_{eff} BCPs.[51–53]

Maintaining a sufficiently low LER is critically important for device performance, and as DSA has approached process integration it is a topic that has received more attention. LER is typically measured by taking critical dimension scanning electron microscopy (CDSEM) images of patterned lines and evaluating the edge fluctuations. The SEM image is converted to a power spectral density, which can be integrated to obtain a $3\sigma_{LER}$, which is typically the figure of merit. In much of the literature the discussion around reducing LER is focused on either process improvement[54] or increased $\chi_{eff.}$[55,56] A comparison of fin field effect transistors (FinFETs) fabricated using either PS-*b*-PMMA or PS-*b*-poly(pentamethyldisilylstyrene) (PS-*b*-PDSS) at 24 nm pitch resulted in a significantly lower LER for PS-*b*-PDSS (1.17 nm vs 2.79 nm for PS-*b*-PMMA), which was the higher χ_{eff} material. The PS-*b*-PDSS system has a significantly higher etch contrast compared gto the PS-*b*-PMMA system due to the silicon in the PDSS block.[22] As a result it is unclear if the origin of the improved LER was the change in χ or the difference in the etching process. Graphoepitaxial patterning of PS-*b*-poly(dimethylsiloxane) (PS-*b*-PDMS) and poly(4-vinylpyridine)-*b*-PDMS (P4VP-*b*-PDMS) resulted in an LER of 2.41 nm and 0.98 nm. In this case the systems are expected to have similar etch contrasts, suggesting that the higher χ_{eff} between P4VP-*b*-PDMS is the driving force for the LER reduction. It is unclear how to directly compare these results to chemoepitaxial based processes, particularly as the BCPs were cylindrical and the confinement in the trench may impact long range fluctuations.[57] To further complicate matters, the template structure itself can impact transfer to the underlying substrate. X-ray measurements have demonstrated that interfacial roughness varies both between lamellae on the guiding stripe and lamellae on the neutral brush, as well as a function of distance from the surface and substrate.[11] Variations in LER between lines on different portions of the guiding template have been experimentally observed.[58]

NIST Author Manuscript

NIST Author Manuscript

NIST Author Manuscript

The impact of additives on BCP structure and thermodynamics have been well established. For systems where the additive is chemically identical to one of the components in the system the distribution will depend on the ratio of the molecular mass between the additive and its identical component in the BCP.[59,60] A-B/C type systems have also been explored, and in many cases are based on hydrogen bonding interactions between the additive and one of the blocks to promote miscibility. In this case the attractive interactions promote uniform distribution of the additive in the resident block regardless of molecular weight.[29–31,61] At low volume fractions the C additive is uniformly distributed throughout its resident phase, as a result the block copolymer must rearrange to accommodate the additive. The interactions will cause the BCP chains in the mixed phase to stretch away from the interface, generally resulting in a reduction in the area per junction (the area occupied by each chain at the interface). Similar trends have been found for the addition of IL to BCPs. Addition of the IL to a lamellar BCP results in an increase in L_O, followed by transitions to cylindrical and spherical phases at sufficiently high concentrations.[25,40,62]

Reflectivity measurements are a common tool for evaluation of the interface width between two phases.[61,63–67] In order to be able to extract w_m, or the thickness of individual layers, there needs to be sufficient contrast between the phases. When using hard X-rays the contrast originates through the difference in the electron density, which for organic materials is often small. In neutron based measurements deuteration of one component can be used to alter the contrast, but this requires synthesizing deuterated components which can be expensive and in some cases impractical. Resonant Soft X-ray reflectivity (RSoXR) provides an opportunity to vary the contrast in thin films by changing the incident energy in the vicinity of an atomic absorption edge. Changing the energy in this region results in a shift in the real (δ) and imaginary (β) components of the complex refractive index (n=1-δ-iβ) which are related through Kramers-Kronig. The contrast (, $=(\delta_1-\delta_2)^2+(\beta_1-\beta_2)^2$) can then be tuned as a function of energy in order to enhance the signal from specific layers or functional groups.[68–71] This approach has been previously utilized to examine blends of PS-*b*-PMMA with a homopolymer (poly(vinylphenol) [PVPH]) which hydrogen bonds to the PMMA block. By varying the contrast the distribution of PVPH was evaluated it was observed that w_m was reduced from the native value of 50 Å to 41 Å at a volume fraction of 0.08.

The potential of DSA using a BCP/IL blend has been previously shown, including demonstrations that with low volumes of IL the DSA pattern can still be prepared with thermal annealing. In order to evaluate the potential of IL/BCP blends for reducing LER in DSA we measured the change in interface width as a function of IL volume fraction (ϕ_{IL}). BCPs with and without an IL additive were patterned using a DSA process and the LER was evaluated through SEM measurements.

Materials and Methods

Materials

[BMPR][TFSI], PS-*b*-PMMA, and the polymer brushes were provided by Tokyo Ohka Kogyo (TOK), Japan.[72] Photoresist AIM5484, Orgsolv STR301 and RER600 were

purchased from JSR Micro, BASF and Fujifilm, respectively. All materials were used as received. The properties of PS-*b*-PMMA are shown in Table 1.

Parallel Lamellae

Parallel lamellae for RSoXR measurements were prepared by spin coating solutions of SM(22.9,22.9)/[BMPR][TFSI] from 4.0–4.2 wt % solutions and a thickness of 5.5 L_0 was controlled by varying the spin coating speed. Optical microscopy was used to check the surface for the presence of island/hole structure. The samples were annealed at 200 °C for 10 min in a nitrogen environment.

Perpendicular Lamellae

P(S-*r*-MMA-*r*-HEMA) with a PS fraction of 0.38 was spun coat from a 0.5% solution and grafted to a bare silicon wafer through a 5 min anneal at 250 °C in a nitrogen atmosphere. The addition of an IL can change the composition window of the neutral brush which leads to perpendicular orientation of the BCP/IL blend. Previous work has shown that this brush composition provides a neutral substrate for the volume fractions of IL investigated in this work.[25] Excess brush was removed via a rinse yielding a 6–7 nm thick brush. SM(39.5,37) and SM(39.5,37)/[BMPR][TFSI] blends (ϕ = 10 wt %) were spun coat from a 1 % solution to target a film thickness of 1 L_0, the samples were then annealed for 5 min at 200 °C in a nitrogen environment.

Directed Self-Assembly

The DSA samples were fabricated on the 300 mm DSA process line in the production cleanroom at imec, Belgium. The chemical patterns were prepared according to a previously reported process on 300 mm Si wafers. An antireflective coating of silicon nitride (SiN) was deposited using a chemical vapor deposition process, The deposited SiN was 13 nm thick, and an 8 nm layer of XPS was deposited on top and crosslinked at 315 °C for 5 min. A photoresist (AIM5484) was coated on the sample (≈ 95 nm thick) using a SOKUDO DUO track and exposed with an ASML 1950 immersion scanner, then developed to yield line-space patters with pitches ranging between 78 nm and 86 nm. Oxygen plasma etch was used to trim the lines and remove unprotected XPS, residual photoresist was stripped with Orgasolv STR301 on a TEL ACT12 track. The pattern was backfilled with P(S-*r*-MMA-*r*-HEMA) and annealed for 5 min at 250 °C under nitrogen. The ungrafted brush was removed and the BCP or BCP/[BMPR][TFSI] was spun coat onto the pattern and annealed for 30 min at 215 °C in a nitrogen environment. PMMA domains were removed using dry etching on a TEL TACTRAS etcher. Hitachi High-Tech CG-5000 was used to capture multiple rectangular scans (0.45 by 2.25 μm^2) of DSA samples post PMMA removal. LER analysis was performed with LER DEMO software licensed from Demokritos National Center of Scientific Research.

Infrared Photoinduced Force Microscopy (IR-PIFM)

A Vistascope (Molecular Vista Inc.) was coupled to a LaserTune QCL. The microscope was operated in dynamic mode using NCH-Au 300 kHz noncontact cantilevers from Nanosensors.

NIST Author Manuscript NIST Author Manuscript NIST Author Manuscript

RSoXR

Resonant soft X-ray reflectivity measurements were conducted at beamline 6.3.2 at the Advanced Light Source at Lawrence Berkeley National Laboratory. Measurements at the carbon edge were conducted with a 600 mm^{-1} grating and Ti filter. The low q data was collected with a photodiode and combined with high q data obtained from a Channeltron. The data was fit using the Refl1d software, using the directed evolution Monte-Carlo Markov Chain algorithm (MCMC).[73] Uncertainties were calculated from the population distribution sampled by the MCMC algorithm, the results presented here represent the 95% confidence intervals. The model includes the underlying silicon and silicon oxide layers. The model constrained all full period layers of PS and PMMA/IL to have equal thickness, and the top/bottom layers to be equal to ½ the full period layer thickness. w_m is calculated according to Equation 1 by fitting the interface width using an error function of width σ.

$$w_M = \sigma\sqrt{2\pi} \tag{1}$$

Results and Discussion

In order to provide initial verification that the [BMPR][TFSI] is located primarily in the PMMA domain IR-PIFM was used to visualize the distribution of the additive. IR-PIFM uses IR absorption of individual components to shift the topological and mechanical properties of the film, enabling direct chemical mapping.[74] Imaging over the same area is conducted using a series of different wavelengths, each targeting an IR absorption band for different components in the film. PS and PMMA were targeted at 1493 cm^{-1} and 1733 cm^{-1}, respectively, while [BMPR][TFSI] was targeted at 1057 cm^{-1}, using the IR spectra shown in the supporting information (SI). Vertical lamellae of native SM(39.5,37) and a blend of SM(39.5,37) with a weight fraction of 10 % [BMPR][TFSI] were prepared and imaged. This molecular weight was used so that the two phases could be clearly resolved in the measurement. Figure 2A shows the image of the native SM(39.5,37) taken using IR at 1057 cm^{-1} (sensitive to the [BMPR][TFSI]), showing no distinct topology. The images of the SM(39.5,37)/[BMPR][TSFI] blend showing a matching behavior at the PMMA and [BMPS][TFSI] wavelengths, while the phase inverts for PS. This result is consistent with the presence of [BMPS][TFSI] in the PMMA phase.

RSoXR measurements were conducted near the carbon edge (280 eV) on SM(22.9,22.9) and SM(22.9,22.9)/[BMPR][TFSI] blends with [BMPR][TFSI] volume fractions ranging from ϕ_{IL} =0 – 0.10, the results of these measurements are shown in Figure 3. The BCPs were oriented parallel to the substrate at a thickness of 5.5 L_0. Polystyrene has a peak in the absorption spectra at ≈ 285 eV, conducting the measurement below the edge takes advantage of the shift in δ without an accompanying increase in β which occurs closer to the edge. The absorption peak for the carbonyl in PMMA takes place closer to 289 eV, as a result the shift in δ for PMMA will be less pronounced at lower energies. 280 eV was therefore chosen as the measurement energy near the carbon edge in order to provide contrast while minimizing beam damage. The reflectivity curves show a multilayer signature, with high frequency fringes corresponding to the total film thickness and long-range modulations of those fringes

NIST Author Manuscript
NIST Author Manuscript
NIST Author Manuscript

indicated by the arrows, which correspond to the BCP periodicity. The rate of decay of those modulations is a function of w_m, with more rapid decay occurring for wider interfaces. Upon addition of the [BMPR][TFSI] the q spacing between the modulations decreases, corresponding to an increasing L_0. The low frequency modulations persist further into q with increasing ionic liquid concentration, this is particularly noticeable for δ_{IL} 0.06, where the 4th order peak becomes more pronounced, and at ϕIL = 0.08 the fifth order peak becomes visible. This indicates a significant reduction in w_m with the addition of larger volume fractions of IL. The composition profiles used to fit the data are shown in the SI. As shown by the IR-PIFM measurements the [BMPR][TFSI] segregates to the PMMA layer and is uniformly distributed (models were used to check for the accumulation of [BMPR][TFSI] at the center of the PMMA layer and resulted in significantly worse fits compared to the uniform distribution model, also shown in SI).

The change in periodicity for each blend series is shown in Figure 4 (4A shows the absolute change in both the PS and PMMA layer thickness, 4B shows the relative change). One of the advantages of examining the BCP multilayers with reflectivity is that the individual layer thicknesses can be reliably determined. The PMMA layer shows a continuous expansion as a function of ϕ_{IL}. The PS layer also expands, faster for $\phi_{IL} < 0.06$ and slower for higher concentrations. This indicates that the IL causes the PMMA chains to stretch away from the interface, resulting in a reduction in the area/junction (shown in the SI). This forces the PS chains to stretch in order to accommodate this rearrangement, which results in the increased layer thickness in spite of the lack of IL in the PS phase. The change in the rate of expansion suggests that the reduction in the area/junction slows with the addition of larger volume fractions of the IL, where the swelling in the lateral direction (relative to the interface) may begin to compete with the chain stretching in the perpendicular direction. This is consistent with previous measurements of AB/C blends where this type of structural change is observed.[30,31] Both experiment and theory have previously determined that $L_0 \sim \phi_\rho^{\alpha}$ (ϕ_ρ is the volume fraction of BCP), where α acts as a measure of solvent selectivity, with more selective solvents resulting in more negative values of α. Fitting this function to the L_0 vs ϕ_{IL} curves results in $\alpha = -1.50$. This is consistent with previous blends of PS-*b*-PMMA and [EMIM]-[TFSI], which found $\alpha \sim 1.6$ in the limit of large N.[62]

The measured w_m is shown in Figure 5A, along with a comparison with literature values of PS-*b*-PMMA/poly(vinyl phenol) (PVPH) blends.[61] The PS-*b*-PMMA/[BMPR][TFSI] series shows a rapid initial decrease in w_m, falling below 35 Å at $\phi_{IL} = 0.04$, this is equivalent to the interface width for PS-*b*-P2VP. w_m continues to decrease with added [BMPR][TFSI], although the majority of the change occurs below $\phi_{IL} = 0.06$, above this value the change in w_m slows considerably. For comparison this is a much larger change than for blends of PS-*b*-PMMA with PVPH, where the PVPH only reduces the interface width to 41 Å at an additive volume fraction of 0.08. From w_m the χ_{eff} between PS and PMMA/[BMPR][TFSI] can be estimated according to Eqs 2–4. In the limit of infinitely long chains the interface width (w_∞) is a function of the statistical segment length (a) and χ_{eff}. This value is then corrected for finite chain length (w_F, Equation 3) and capillary wave fluctuations (w_P, Equation 4).[57,75] From this estimation PS-*b*-PMMA/[BMPR][TFSI] reaches $\chi_{eff} = 0.134$ at $\phi_{IL} = 0.1$, well above what is achieved with the PS-*b*-PMMA/PVPH blend ($\chi_{eff} = 0.056$ at a volume fraction of 0.08). The origin of the difference between the two types of additives is

NIST Author Manuscript NIST Author Manuscript NIST Author Manuscript

not immediately clear. It is also known that only a fraction of the monomers of PVPH participate in hydrogen bonding, possible due to conformation restrictions, which could weaken the impact.[31] The IL is free of such restrictions and can configure as needed to minimize the free energy of the system. Similar shifts in χ_{eff} to the IL blends have been achieved between bilayers of PS and PMMA/PVPH, but require PVPH volume fractions of upwards of 0.3, which would drive an order-order transition to a cylindrical phase in a BCP. From these results it is clear the IL has significant advantages over the homopolymer additive in terms of the magnitude of the change in the w_{m} and χ_{eff}.

$$w_{\infty} = \frac{2a}{\sqrt{6\chi_{e}ff}} \tag{2}$$

$$w_F = w_{\infty}\left[1 + 1.34(\chi_{eff}N)^{-1/3}\right] \tag{3}$$

$$w_P = \left[w_F{}^2 + \frac{3vw_{\infty}}{a^2}ln(L/w_{\infty})\right]^{1/2} \tag{4}$$

A potentially useful metric in evaluating a system for DSA is the ratio of w_{m} to L_0, which describes how much of the BCP is composed of the interface region. In Figure 6 w_{m}/L_0 is plotted as a function of $\chi_{\text{eff}}N$ along with results from a series of BCPs with χ_{eff} ranging from ≈ 0.045 –0.25.[67] This series is shifted to slightly lower $w\text{m}/L_0$ compared to the native BCPs measured in the previous study, but the scaling relationship ($w_{\text{m}}/L0 \sim (\chi_{\text{eff}}N)^{\omega}$) follows a similar power law dependence, where ω = –0.6 a nearly identical to the previous data (ω = –2/3 for $\chi_{\text{eff}}N > 35$). In this system the reduction in w_{m} significantly outpaces L_0 growth, resulting in interface fractions that are comparable to BCPs with much higher native χ_{eff}.

An increase in χ_{eff} is expected to result in a reduction in LER for BCPs patterned in line-space arrays via the DSA process. The previous studies that have examined this hypothesis utilized systems where one of the components consisted of a silicon containing polymer, and as a result there was significant difference in the etch resistance between the two components and the contributions from χ_{eff} could not be isolated. To test whether a change in χ_{eff} alone was sufficient to reduce LER we prepared a DSA patterns and assembled three different BCP systems on the same template. The BCPs included SM(22.9,22.9), SM(30.4,27.4) and SM(22.9,22.9)/[BMPR][TFSI] at $\delta_{\text{IL}} = 0.08$, this series was chosen in order to compare the blended sample both to its native BCP and to a PS-*b*-PMMA system with nearly equal pitch. The IL volume fraction was chosen so that the L_0 of the BCP blend would be commensurate with the pitch of the template pattern. Significant deviations of the BCP L_0 from the template pattern are known to influence LER.[76] The resulting patterns were measured with CDSEM after PMMA was removed and representative images are shown in Figure 7A, with the corresponding power spectral density (PSD) curves shown in Figure 7B. The curves show little change between the three samples, with only a slight reduction in the low frequency roughness for the blended samples. The area under the PSD curve can be converted to $3\sigma_{\text{LER}}$, which was found to be 2.88 nm for SM(22.9,22.9), 2.76

NIST Author Manuscript NIST Author Manuscript NIST Author Manuscript

nm for SM(30.4,27.4) and 2.67 nm for SM(22.9,22.9)/[BMPR][TFSI]. $3\sigma_{LER}$ and normalized $3\sigma_{LER}$ ($3\sigma_{LER}/L_0$) are shown in the inset as a function of $\chi_{eff}N$. These results show that in spite of the significant change in χ_{eff} and w_m when [BMPR][TFSI] is added to PS-*b*-PMMA this results in only a small change in LER.

This result stands in contrast to the high χ_{eff} polymers that were discussed previously, where the increase in χ_{eff} leads to a reduction in LER.[55,56] There are two potential origins of the divergence in these results. The first possibility is that the presence of the additive prevents the LER reduction. Modeling shown in the SI shows that the IL is uniformly distributed throughout the PMMA block, reducing the possibility that this is caused by heterogeneities in the IL distribution. The IL will also impact the properties of the PMMA block, such as the glass transition temperature (T_g) and segmental mobility. Changes in the mechanical properties of the polymer driven by these shifts could be a contributing factor. Studies of PMMA blended with 1-ethyl-3-methylimidazolium bis(trifluoromethylsulfonyl)imide show reduced T_g and a shift in the mechanical response towards more liquid-like behavior.[77] The other possibility is that the increase in χ_{eff} alone is insufficient to change the LER and that it must be coupled with a higher etch contrast. In every case where the change in χ_{eff} led to reduced LER the etch contrast was enhanced by the presence of silicon in one of the blocks. This suggests that a more promising design strategy for high χ_{eff} systems is to focus on materials with larger intrinsic etch contrast.

Conclusions

Blending additives is a promising strategy to produce higher χ_{eff} systems, but as shown here the change in χ_{eff} may not lead to lower LER in a DSA patterned system. Adding ([BMPR][TFSI]) to PS-*b*-PMMA resulted in reduced interface widths in parallel lamellae as a result of the increase in χ_{eff}. This result was directly related to changes in LER between PS-*b*-PMMA and a PS-*b*-PMMA/[BMPR][TFSI] blend, where negligible changes in LER were observed upon removal of the PMMA/IL block. This contrasts with previous results which interrogated DSA patterned BCP systems which had a higher native etch contrast. These results show that both increased etch contrast and χ_{eff} will likely be necessary to reduce LER to levels required for optimum device performance, particularly in the case of sub-10 nm periodicities. To better understand this result companion experiments could be performed on all-organic high χ_{eff} polymers, using sequential infiltration synthesis to control the etch contrast between the BCP components. This type of experiment would complement the results of this study by better quantifying the relationship between etch contrast and LER.

Supplementary Material

Refer to Web version on PubMed Central for supplementary material.

Acknowledgements

This work was supported by award 70NHNB14H012 from the U.S. Department of Commerce, National Institute of Standards and Technology, as part of the Center for Hierarchical Materials Design (CHiMaD). The Advanced Light Source is supported by the Director, Office of Science, Office of Basic Energy Sciences, of the U.S. Department of

NIST Author Manuscript
NIST Author Manuscript
NIST Author Manuscript

Energy under Contract No. DE-AC02-05CH11231. We thank Eric Gullikson for assistance at BL. 6.3.2. and Paul Kienzle for the work developing the Refl1D software.

References

(1). Raley A; Mack CA; Liu E; Thibaut S; Ko A Benchmarking of EUV Lithography Line/Space Patterning versus Immersion Lithography Multipatterning Schemes at Equivalent Pitch In International Conference on Extreme Ultraviolet Lithography 2018; Ronse KG, Gargini PA, Hendrickx E, Naulleau PP, Itani T, Eds.; SPIE: Monterey, United States, 2018; p 1080915 10.1117/12.2501680.

(2). van Veenhuizen M; Allen G; Harmes M; Indukuri T; Jezewski C; Krist B; Lang H; Myers A; Schenker R; Singh KJ Demonstration of an Electrically Functional 34 Nm Metal Pitch Interconnect in Ultralow-k ILD Using Spacer-Based Pitch Quartering In Proc. IEEE; IEEE: San Jose, California, USA, 2012; pp 1–3. 10.1109/IITC.2012.6251665.

(3). Kono T; Hatano M; Tokue H; Kato H; Fukuhara K; Nakasugi T Half-Pitch 14nm Direct Patterning with Nanoimprint Lithography In Novel Patterning Technologies for Semiconductors, MEMS/NEMS, and MOEMS 2019; Panning EM, Sanchez MI, Eds.; SPIE: San Jose, United States, 2019; p 10958OH 10.1117/12.2514685.

(4). Kim SO; Solak HH; Stoykovich MP; Ferrier NJ; de Pablo JJ; Nealey PF Epitaxial Self-Assembly of Block Copolymers on Lithographically Defined Nanopatterned Substrates. Nature 2003, 424 (6947), 411–414. 10.1038/nature01775. [PubMed: 12879065]

(5). Stoykovich MP Directed Assembly of Block Copolymer Blends into Nonregular Device-Oriented Structures. Science 2005, 308 (5727), 1442–1446. 10.1126/science.1111041. [PubMed: 15933196]

(6). Williamson LD; Seidel RN; Chen X; Suh HS; Rincon Delgadillo P; Gronheid R; Nealey PF Three-Tone Chemical Patterns for Block Copolymer Directed Self-Assembly. ACS Appl. Mater. Interfaces 2016, 8 (4), 2704–2712. 10.1021/acsami.5b10562. [PubMed: 26742859]

(7). Cushen J; Wan L; Blachut G; Maher MJ; Albrecht TR; Ellison CJ; Willson CG; Ruiz R Double-Patterned Sidewall Directed Self-Assembly and Pattern Transfer of Sub-10 Nm PTMSS- *b* -PMOST. ACS Appl. Mater. Interfaces 2015, 7 (24), 13476–13483. 10.1021/acsami.5b02481. [PubMed: 26004013]

(8). Muramatsu M; Nishi T; You G; Ido Y; Kitano T Pattern Defect Reduction for Chemo-Epitaxy DSA Process In Advances in Patterning Materials and Processes XXXVI; Gronheid R, Sanders DP, Eds.; SPIE: San Jose, United States, 2019; p 109600W 10.1117/12.2514671.

(9). Muramatsu M; Nishi T; You G; Saito Y; Ido Y; Oikawa N; Tobana T; Ito K; Morikita S; Kitano T Pattern Defect Reduction and LER Improvement of Chemo-Epitaxy DSA Process In Emerging Patterning Technologies; Bencher C, Cheng JY, Eds.; San Jose, California, United States, 2017; p 101440Q 10.1117/12.2257952.

(10). Li J; Rincon-Delgadillo PA; Suh HS; Mannaert G; Nealey PF Kinetics of Defect Annihilation in Chemo-Epitaxy Directed Self-Assembly In Advances in Patterning Materials and Processes XXXVI; Gronheid R, Sanders DP, Eds.; SPIE: San Jose, United States, 2019; p 109600V 10.1117/12.2514731.

(11). Khaira G; Doxastakis M; Bowen A; Ren J; Suh HS; Segal-Peretz T; Chen X; Zhou C; Hannon AF; Ferrier NJ; et al. Derivation of Multiple Covarying Material and Process Parameters Using Physics-Based Modeling of X-Ray Data. Macromolecules 2017, 50 (19), 7783–7793. 10.1021/acs.macromol.7b00691.

(12). Sinturel C; Bates FS; Hillmyer MA High?–Low *N* Block Polymers: How Far Can We Go? ACS Macro Lett 2015, 4 (9), 1044–1050. 10.1021/acsmacrolett.5b00472.

(13). Kwak J; Mishra AK; Lee J; Lee KS; Choi C; Maiti S; Kim M; Kim JK Fabrication of Sub-3 Nm Feature Size Based on Block Copolymer Self-Assembly for Next-Generation Nanolithography. Macromolecules 2017, 50 (17), 6813–6818. 10.1021/acs.macromol.7b00945.

(14). Jeong G; Yu DM; Mapas JKD; Sun Z; Rzayev J; Russell TP Realizing 5.4 Nm Full Pitch Lamellar Microdomains by a Solid-State Transformation. Macromolecules 2017, 50 (18), 7148–7154. 10.1021/acs.macromol.7b01443.

NIST Author Manuscript NIST Author Manuscript NIST Author Manuscript

(15). Carter MCD; Jennings J; Speetjens FW; Lynn DM; Mahanthappa MK A Reactive Platform Approach for the Rapid Synthesis and Discovery of High χ/Low *N* Block Polymers. Macromolecules 2016, 49 (17), 6268–6276. 10.1021/acs.macromol.6b01268.

(16). Zhou SX; Janes DW; Kim CB; Willson CG; Ellison CJ Designing Intrablock Attractions To Increase the χ Parameter of a Symmetric Diblock Copolymer. Macromolecules 2016 10.1021/acs.macromol.6b01382.

(17). Kanimozhi C; Kim M; Larson SR; Choi JW; Choo Y; Sweat DP; Osuji CO; Gopalan P Isomeric Effect Enabled Thermally Driven Self-Assembly of Hydroxystyrene-Based Block Copolymers. ACS Macro Lett 2016, 5 (7), 833–838. 10.1021/acsmacrolett.6b00376.

(18). Yao L; Oquendo LE; Schulze MW; Lewis RM; Gladfelter WL; Hillmyer MA Poly(Cyclohexylethylene)- *Block* -Poly(Lactide) Oligomers for Ultrasmall Nanopatterning Using Atomic Layer Deposition. ACS Appl. Mater. Interfaces 2016, 8 (11), 7431–7439. 10.1021/acsami.5b12785. [PubMed: 26954771]

(19). Minehara H; Pitet LM; Kim S; Zha RH; Meijer EW; Hawker CJ Branched Block Copolymers for Tuning of Morphology and Feature Size in Thin Film Nanolithography. Macromolecules 2016, 49 (6), 2318–2326. 10.1021/acs.macromol.5b02649.

(20). Vora A; Wojtecki RJ; Schmidt K; Chunder A; Cheng JY; Nelson A; Sanders DP Development of Polycarbonate-Containing Block Copolymers for Thin Film Self-Assembly Applications. Polym Chem 2016, 7 (4), 940–950. 10.1039/C5PY01846C.

(21). Shi W; Tateishi Y; Li W; Hawker CJ; Fredrickson GH; Kramer EJ Producing Small Domain Features Using Miktoarm Block Copolymers with Large Interaction Parameters. ACS Macro Lett 2015, 4 (11), 1287–1292. 10.1021/acsmacrolett.5b00712.

(22). Durand WJ; Blachut G; Maher MJ; Sirard S; Tein S; Carlson MC; Asano Y; Zhou SX; Lane AP; Bates CM; et al. Design of High-χ Block Copolymers for Lithography. J. Polym. Sci. Part Polym. Chem 2015, 53 (2), 344–352. 10.1002/pola.27370.

(23). Liu C-C; Franke E; Mignot Y; Xie R; Yeung CW; Zhang J; Chi C; Zhang C; Farrell R; Lai K; et al. Directed Self-Assembly of Block Copolymers for 7 Nanometre FinFET Technology and Beyond. Nat. Electron 2018, 1 (10), 562–569. 10.1038/s41928-018-0147-4.

(24). Pang Y; Jin X; Huang G; Wan L; Ji S Directed Self-Assembly of Styrene-Methyl Acrylate Block Copolymers with Sub-7 Nm Features via Thermal Annealing. Macromolecules 2019, 2987–2994. 10.1021/acs.macromol.9b00174.

(25). Chen X; Zhou C; Chen S-J; Craig GSW; Rincon-Delgadillo P; Dazai T; Miyagi K; Maehashi T; Yamazaki A; Gronheid R; et al. Ionic Liquids as Additives to Polystyrene- *Block* -Poly(Methyl Methacrylate) Enabling Directed Self-Assembly of Patterns with Sub-10 Nm Features. ACS Appl. Mater. Interfaces 2018, 10 (19), 16747–16759. 10.1021/acsami.8b02990. [PubMed: 29667409]

(26). Pimenta Barros P; Barnola S; Gharbi A; Argoud M; Servin I; Tiron R; Chevalier X; Navarro C; Nicolet C; Lapeyre C; et al. Etch Challenges for DSA Implementation in CMOS via Patterning In Advanced Etch Technology for Nanopatterning III,; SPIE: San Jose, California, USA, 2014; p 90540G 10.1117/12.2046267.

(27). Tirumala VR; Romang A; Agarwal S; Lin EK; Watkins JJ Well Ordered Polymer Melts from Blends of Disordered Triblock Copolymer Surfactants and Functional Homopolymers. Adv. Mater. 2008, 20 (9), 1603–1608. 10.1002/adma.200701577.

(28). Dobrosielska K; Wakao S; Suzuki J; Noda K; Takano A; Matsushita Y Effect of Homopolymer Molecular Weight on Nanophase-Separated Structures of AB Block Copolymer/C Homopolymer Blends with Hydrogen-Bonding Interactions. Macromolecules 2009, 42 (18), 7098–7102. 10.1021/ma901212p.

(29). Bosse AW; Tirumala VR; Lin EK Tuning Block Copolymer Phase Behavior with a Selectively Associating Homopolymer Additive. J. Polym. Sci. Part B Polym. Phys. 2009, 47 (21), 2083–2090. 10.1002/polb.21805.

(30). Sunday DF; Hannon AF; Tein S; Kline RJ Thermodynamic and Morphological Behavior of Block Copolymer Blends with Thermal Polymer Additives. Macromolecules 2016, 49 (13), 4898–4908. 10.1021/acs.macromol.6b00651.

NIST Author Manuscript

NIST Author Manuscript

NIST Author Manuscript

(31). Chen S-C; Kuo S-W; Jeng U-S; Su C-J; Chang F-C On Modulating the Phase Behavior of Block Copolymer/Homopolymer Blends via Hydrogen Bonding. Macromolecules 2010, 43 (2), 1083–1092. 10.1021/ma901729t.

(32). Wang J; Odarchenko YI; Defaux M; Lejnieks J; Ahokhin DV; Keul H; Ivanov DA; Möller M; Mourran A Concurrent Order in a Semi-Crystalline Diblock Copolymer Involving Complexation with a Mesogen. Macromolecules 2013, 46 (15), 6159–6168. 10.1021/ma4008797.

(33). Yao L; Lu X; Chen S; Watkins JJ Formation of Helical Phases in Achiral Block Copolymers by Simple Addition of Small Chiral Additives. Macromolecules 2014, 47 (19), 6547–6553. 10.1021/ma501714g.

(34). Daga VK; Watkins JJ Hydrogen-Bond-Mediated Phase Behavior of Complexes of Small Molecule Additives with Poly(Ethylene Oxide- *b* -Propylene Oxide- *b* -Ethylene Oxide) Triblock Copolymer Surfactants. Macromolecules 2010, 43 (23), 9990–9997. 10.1021/ma101694n.

(35). Daga VK; Anderson ER; Gido SP; Watkins JJ Hydrogen Bond Assisted Assembly of Well-Ordered Polyhedral Oligomeric Silsesquioxane—Block Copolymer Composites. Macromolecules 2011, 44 (17), 6793–6799. 10.1021/ma200926n.

(36). Gartner TE; Kubo T; Seo Y; Tansky M; Hall LM; Sumerlin BS; Epps TH Domain Spacing and Composition Profile Behavior in Salt-Doped Cyclic vs Linear Block Polymer Thin Films: A Joint Experimental and Simulation Study. Macromolecules 2017, 50 (18), 7169–7176. 10.1021/acs.macromol.7b01338.

(37). Thelen JL; Teran AA; Wang X; Garetz BA; Nakamura I; Wang Z-G; Balsara NP Phase Behavior of a Block Copolymer/Salt Mixture through the Order-to-Disorder Transition. Macromolecules 2014, 47 (8), 2666–2673. 10.1021/ma500292n.

(38). Teran AA; Balsara NP Thermodynamics of Block Copolymers with and without Salt. J. Phys. Chem. B 2014, 118 (1), 4–17. 10.1021/jp408079z. [PubMed: 24229067]

(39). Virgili JM; Hoarfrost ML; Segalman RA Effect of an Ionic Liquid Solvent on the Phase Behavior of Block Copolymers. Macromolecules 2010, 43 (12), 5417–5423. 10.1021/ma902804e.

(40). Miranda DF; Russell TP; Watkins JJ Ordering in Mixtures of a Triblock Copolymer with a Room Temperature Ionic Liquid. Macromolecules 2010, 43 (24), 10528–10535. 10.1021/ma1015209.

(41). Bennett TM; Pei K; Cheng H-H; Thurecht KJ; Jack KS; Blakey I Can Ionic Liquid Additives Be Used to Extend the Scope of Poly (Styrene)-Block-Poly (Methyl Methacrylate) for Directed Self-Assembly? J. MicroNanolithography MEMS MOEMS 2014, 13 (3), 031304–031304. 10.1117/1.JMM.13.3.031304.

(42). Tiron R; Chevalier X; Couderc C; Pradelles J; Bustos J; Pain L; Navarro C; Magnet S; Fleury G; Hadziioannou G Optimization of Block Copolymer Self-Assembly through Graphoepitaxy: A Defectivity Study. J. Vac. Sci. Technol. B Microelectron. Nanometer Struct. 2011, 29 (6), 06F206 10.1116/1.3659714.

(43). Graves T; Vaglio Pret A; Robertson S; Smith M; Doise J; Bekaert J; Gronheid R DSA Graphoepitaxy Calibrations for Contact Hole Multiplication In Proc. SPIE; Wallow TI, Hohle CK, Eds.; SPIE: San Jose, California, USA, 2015; p 94250Y 10.1117/12.2086137.

(44). Liu C-C; Ramírez-Hernández A; Han E; Craig GSW; Tada Y; Yoshida H; Kang H; Ji S; Gopalan P; de Pablo JJ; et al. Chemical Patterns for Directed Self-Assembly of Lamellae-Forming Block Copolymers with Density Multiplication of Features. Macromolecules 2013, 46 (4), 1415–1424. 10.1021/ma302464n.

(45). Wan L; Ji S; Liu C-C; Craig GSW; Nealey PF Directed Self-Assembly of Solvent-Vapor-Induced Non-Bulk Block Copolymer Morphologies on Nanopatterned Substrates. Soft Matter 2016, 12 (11), 2914–2922. 10.1039/C5SM02829A. [PubMed: 26891026]

(46). Jeong JW; Park WI; Kim M-J; Ross CA; Jung YS Highly Tunable Self-Assembled Nanostructures from a Poly(2-Vinylpyridine- *b* -Dimethylsiloxane) Block Copolymer. Nano Lett 2011, 11 (10), 4095–4101. 10.1021/nl2016224. [PubMed: 21950245]

(47). Bates CM; Seshimo T; Maher MJ; Durand WJ; Cushen JD; Dean LM; Blachut G; Ellison CJ; Willson CG Polarity-Switching Top Coats Enable Orientation of Sub-10-Nm Block Copolymer Domains. Science 2012, 338 (6108), 775–779. 10.1126/science.1226046. [PubMed: 23139327]

(48). Suh HS; Kim DH; Moni P; Xiong S; Ocola LE; Zaluzec NJ; Gleason KK; Nealey PF Sub-10-Nm Patterning via Directed Self-Assembly of Block Copolymer Films with a Vapour-Phase

NIST Author Manuscript

NIST Author Manuscript

NIST Author Manuscript

Deposited Topcoat. Nat. Nanotechnol 2017, 12 (6), 575–581. 10.1038/nnano.2017.34. [PubMed: 28346456]

(49). Tseng Y-C; Peng Q; Ocola LE; Czaplewski DA; Elam JW; Darling SB Etch Properties of Resists Modified by Sequential Infiltration Synthesis. J. Vac. Sci. Technol. B Microelectron. Nanometer Struct. 2011, 29 (6), 06FG01 10.1116/1.3640758.

(50). Lane AP; Yang X; Maher MJ; Blachut G; Asano Y; Someya Y; Mallavarapu A; Sirard SM; Ellison CJ; Willson CG Directed Self-Assembly and Pattern Transfer of Five Nanometer Block Copolymer Lamellae. ACS Nano 2017, 11, 7656 10.1021/acsnano.7b02698. [PubMed: 28700207]

(51). Jiang J; Jacobs AG; Wenning B; Liedel C; Thompson MO; Ober CK Ultrafast Self-Assembly of Sub-10 Nm Block Copolymer Nanostructures by Solvent-Free High-Temperature Laser Annealing. ACS Appl. Mater. Interfaces 2017, 9 (37), 31317–31324. 10.1021/acsami.7b00774. [PubMed: 28598156]

(52). Jin HM; Lee SH; Kim JY; Son S-W; Kim BH; Lee HK; Mun JH; Cha SK; Kim JS; Nealey PF; et al. Laser Writing Block Copolymer Self-Assembly on Graphene Light-Absorbing Layer. ACS Nano 2016, 10 (3), 3435–3442. 10.1021/acsnano.5b07511. [PubMed: 26871736]

(53). Jin HM; Park DY; Jeong S-J; Lee GY; Kim JY; Mun JH; Cha SK; Lim J; Kim JS; Kim KH; et al. Flash Light Millisecond Self-Assembly of High? Block Copolymers for Wafer-Scale Sub-10 Nm Nanopatterning. Adv. Mater 2017, 29 (32), 1700595 10.1002/adma.201700595.

(54). Xiong S; Chapuis Y-A; Wan L; Gao H; Li X; Ruiz R; Nealey PF Directed Self-Assembly of High-Chi Block Copolymer for Nano Fabrication of Bit Patterned Media via Solvent Annealing. Nanotechnology 2016, 27 (41), 415601 10.1088/0957-4484/27/41/415601. [PubMed: 27606926]

(55). Tsai H; Miyazoe H; Vora A; Magbitang T; Arellano N; Liu C-C; Maher MJ; Durand WJ; Dawes SJ; Bucchignano JJ; et al. High Chi Block Copolymer DSA to Improve Pattern Quality for FinFET Device Fabrication In Proc. SPIE; Hohle CK, Younkin TR, Eds.; SPIE: San Jose, California, United States, 2016; p 977910 10.1117/12.2219544.

(56). Kim JM; Hur YH; Jeong JW; Nam TW; Lee JH; Jeon K; Kim Y; Jung YS Block Copolymer with an Extremely High Block-to-Block Interaction for a Significant Reduction of Line-Edge Fluctuations in Self-Assembled Patterns. Chem. Mater. 2016 10.1021/acs.chemmater.6b01731.

(57). Sferrazza M; Xiao C; Jones RAL; Bucknall DG; Webster J; Penfold J Evidence for Capillary Waves at Immiscible Polymer/Polymer Interfaces. Phys. Rev. Lett. 1997, 78 (19), 3693–3966. 10.1103/PhysRevLett.78.3693.

(58). Blachut G; Sirard SM; Hymes D; Mack CA; Maher MJ; Rincon-Delgadillo PA; Chan BT; Mannaert G; Vandenberghe G; Willson G; et al. Evolution of Roughness during the Pattern Transfer of High-Chi, 10nm Half-Pitch, Silicon-Containing Block Copolymer Structures In Advanced Etch Technology for Nanopatterning VII; Engelmann SU, Wise RS, Eds.; SPIE: San Jose, United States, 2018; p 1058907 10.1117/12.2297489.

(59). Winey KI; Thomas EL; Fetters LJ Swelling of Lamellar Diblock Copolymer by Homopolymer: Influences of Homopolymer Concentration and Molecular Weight. Macromolecules 1991, 24 (23), 6182–6188. 10.1021/ma00023a020.

(60). Tanaka H; Hasegawa H; Hashimoto T Ordered Structure in Mixtures of a Block Copolymer and Homopolymers. 1. Solubilization of Low Molecular Weight Homopolymers. Macromolecules 1991, 24 (1), 240–251. 10.1021/ma00001a037.

(61). Sunday DF; Kline RJ Reducing Block Copolymer Interfacial Widths through Polymer Additives. Macromolecules 2015, 48 (3), 679–686. 10.1021/ma502015u.

(62). Bennett TM; Jack KS; Thurecht KJ; Blakey I Perturbation of the Experimental Phase Diagram of a Diblock Copolymer by Blending with an Ionic Liquid. Macromolecules 2016, 49 (1), 205–214. 10.1021/acs.macromol.5b02041.

(63). Anastasiadis SH; Russell TP; Satija SK; Majkrzak CF Neutron Reflectivity Studies of the Surface-Induced Ordering of Diblock Copolymer Films. Phys. Rev. Lett. 1989, 62 (16), 1852–1855. 10.1103/PhysRevLett.62.1852. [PubMed: 10039787]

(64). Longanecker M; Modi A; Dobrynin A; Kim S; Yuan G; Jones R; Satija S; Bang J; Karim A Reduced Domain Size and Interfacial Width in Fast Ordering Nanofilled Block Copolymer Films

NIST Author Manuscript
NIST Author Manuscript
NIST Author Manuscript

by Direct Immersion Annealing. Macromolecules 2016, 49 (22), 8563–8571. 10.1021/acs.macromol.6b01690.

(65). Lin EK Direct Measurement of the Reaction Front in Chemically Amplified Photoresists. Science 2002, 297 (5580), 372–375. 10.1126/science.1072092. [PubMed: 12130778]

(66). Russell TP; Menelle A; Hamilton WA; Smith GS; Satija SK; Majkrzak CF Width of Homopolymer Interfaces in the Presence of Symmetric Diblock Copolymers. Macromolecules 1991, 24 (20), 5721–5726. 10.1021/ma00020a036.

(67). Sunday DF; Maher MJ; Hannon AF; Liman CD; Tein S; Blachut G; Asano Y; Ellison CJ; Willson CG; Kline RJ Characterizing the Interface Scaling of High χ Block Copolymers near the Order–Disorder Transition. Macromolecules 2018, 51 (1), 173–180. 10.1021/acs.macromol.7b01982. [PubMed: 29706666]

(68). Ade H; Wang C; Garcia A; Yan H; Sohn KE; Hexemer A; Bazan GC; Nguyen T-Q; Kramer EJ Characterization of Multicomponent Polymer Trilayers with Resonant Soft X-Ray Reflectivity. J. Polym. Sci. Part B Polym. Phys. 2009, 47 (13), 1291–1299. 10.1002/polb.21730.

(69). Sunday DF; Chang AB; Liman CD; Gann E; Delongchamp DM; Thomsen L; Matsen MW; Grubbs RH; Soles CL Self-Assembly of ABC Bottlebrush Triblock Terpolymers with Evidence for Looped Backbone Conformations. Macromolecules 2018, 51 (18), 7178–7185. 10.1021/acs.macromol.8b01370.

(70). Macke S; Radi A; Hamann-Borrero JE; Bluschke M; Brück S; Goering E; Sutarto R; He F; Cristiani G; Wu M; et al. Element Specific Monolayer Depth Profiling. Adv. Mater. 2014, 26 (38), 6554–6559. 10.1002/adma.201402028. [PubMed: 25103570]

(71). Sunday DF; Chan EP; Orski SV; Nieuwendaal RC; Stafford CM Functional Group Quantification of Polymer Nanomembranes with Soft X-Rays. Phys. Rev. Mater. 2018, 2 (3). 10.1103/PhysRevMaterials.2.032601.

(72). Certain Commercial Equipment, Instruments, or Materials Are Identified in This Paper in Order to Specify the Experimental Procedure Adequately. Such Identification Is Not Intended to Imply Recommendation or Endorsement by the National Institute of Standards and Technology, nor Is It Intended to Imply That the Materials or Equipment Identified Are Necessarily the Best Available for the Purpose.

(73). Vrugt JA; Ter Braak CJF DREAM_(D): An Adaptive Markov Chain Monte Carlo Simulation Algorithm to Solve Discrete, Noncontinuous, and Combinatorial Posterior Parameter Estimation Problems. Hydrol. Earth Syst. Sci 2011, 15 (12), 3701–3713. 10.5194/hess-15-3701-2011.

(74). Nowak D; Morrison W; Wickramasinghe HK; Jahng J; Potma E; Wan L; Ruiz R; Albrecht TR; Schmidt K; Frommer J; et al. Nanoscale Chemical Imaging by Photoinduced Force Microscopy. Sci. Adv 2016, 2 (3), e1501571 10.1126/sciadv.1501571. [PubMed: 27051870]

(75). Semenov AN Theory of Block Copolymer Interfaces in the Strong Segregation Limit. Macromolecules 1993, 26 (24), 6617–6621. 10.1021/ma00076a047.

(76). Sunday DF; Ashley E; Wan L; Patel KC; Ruiz R; Kline RJ Template-Polymer Commensurability and Directed Self-Assembly Block Copolymer Lithography. J. Polym. Sci. Part B Polym. Phys. 2015, 53 (8), 595–603. 10.1002/polb.23675.

(77). Mok MM; Liu X; Bai Z; Lei Y; Lodge TP Effect of Concentration on the Glass Transition and Viscoelastic Properties of Poly(Methyl Methacrylate)/Ionic Liquid Solutions. Macromolecules 2011, 44 (4), 1016–1025. 10.1021/ma102503j.

NIST Author Manuscript

NIST Author Manuscript

NIST Author Manuscript

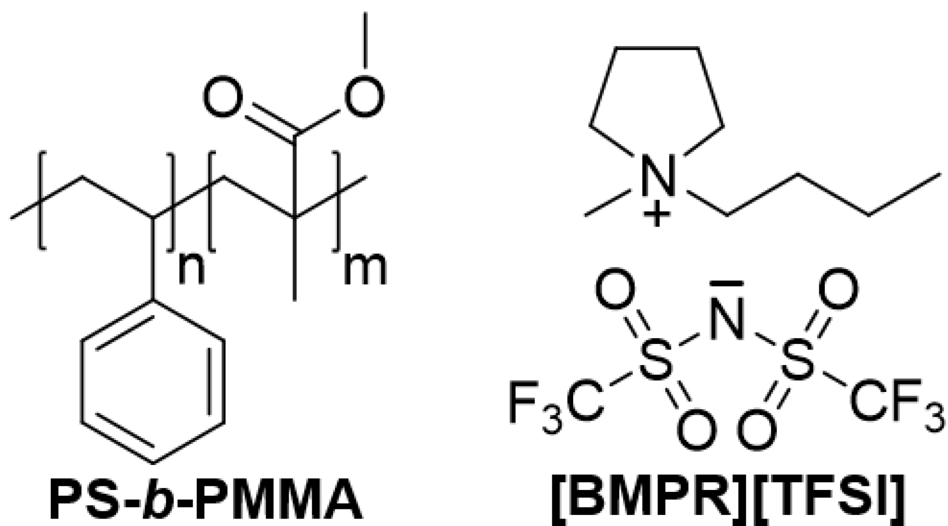

Figure 1:
Structure of the polymer and ionic liquid, N-butyl-N-methylpyrrolidinium bis(trifluoromethylsulfonyl)imide ([BMPR][TFSI]), used in this study.

NIST Author Manuscript

NIST Author Manuscript

NIST Author Manuscript

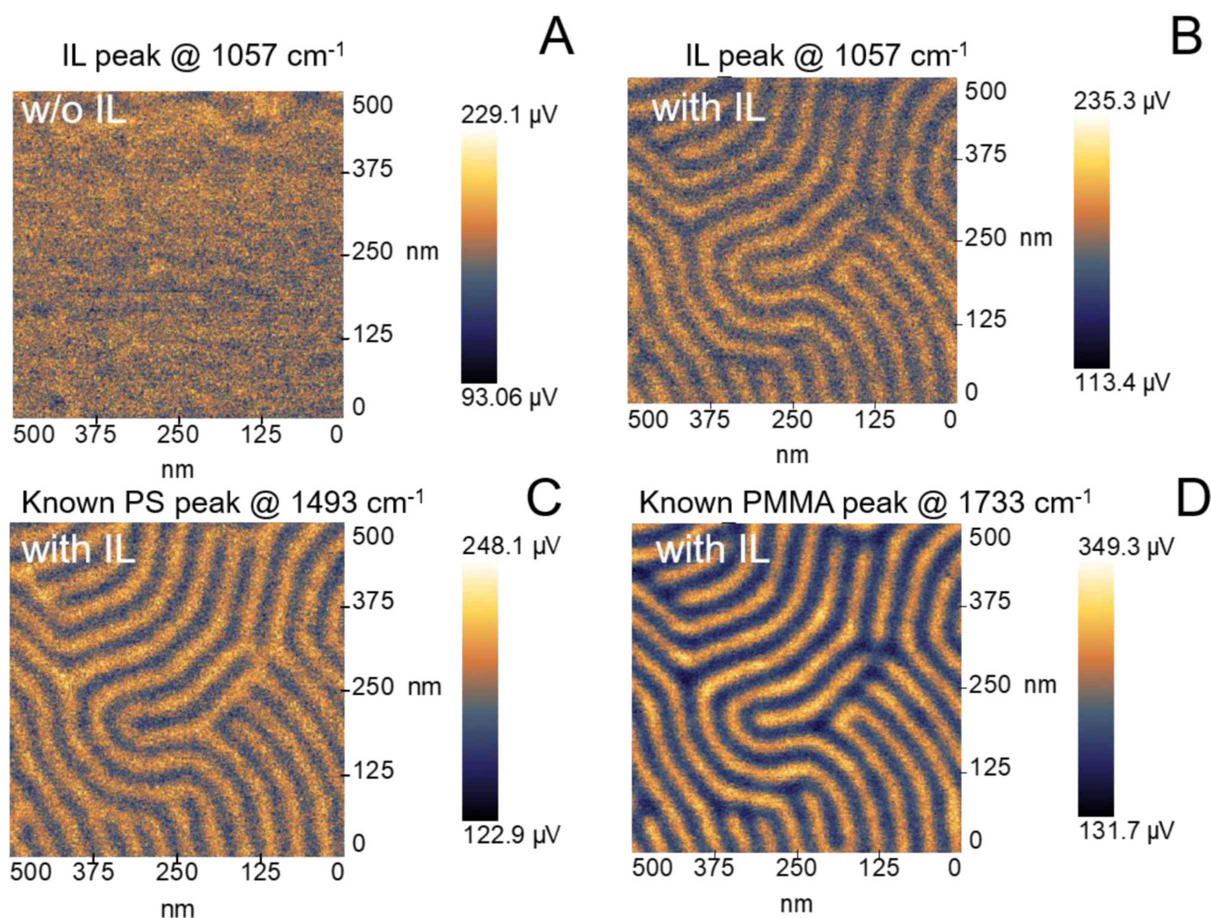

Figure 2:

IR-PIFM images of a) SM (39.5, 37) at 1057 cm^{-1}; b) SM (39.5, 37) and [BMPR][TFSI] blends at 1057 cm^{-1}; c) 1493 cm^{-1}; and d) 1733 cm^{-1}. Wavenumbers of 1057 cm^{-1}, 1493 cm^{-1} and 1733 cm^{-1} correspond to the adsorption peaks of IL, PS and PMMA respectively.

NIST Author Manuscript

NIST Author Manuscript

NIST Author Manuscript

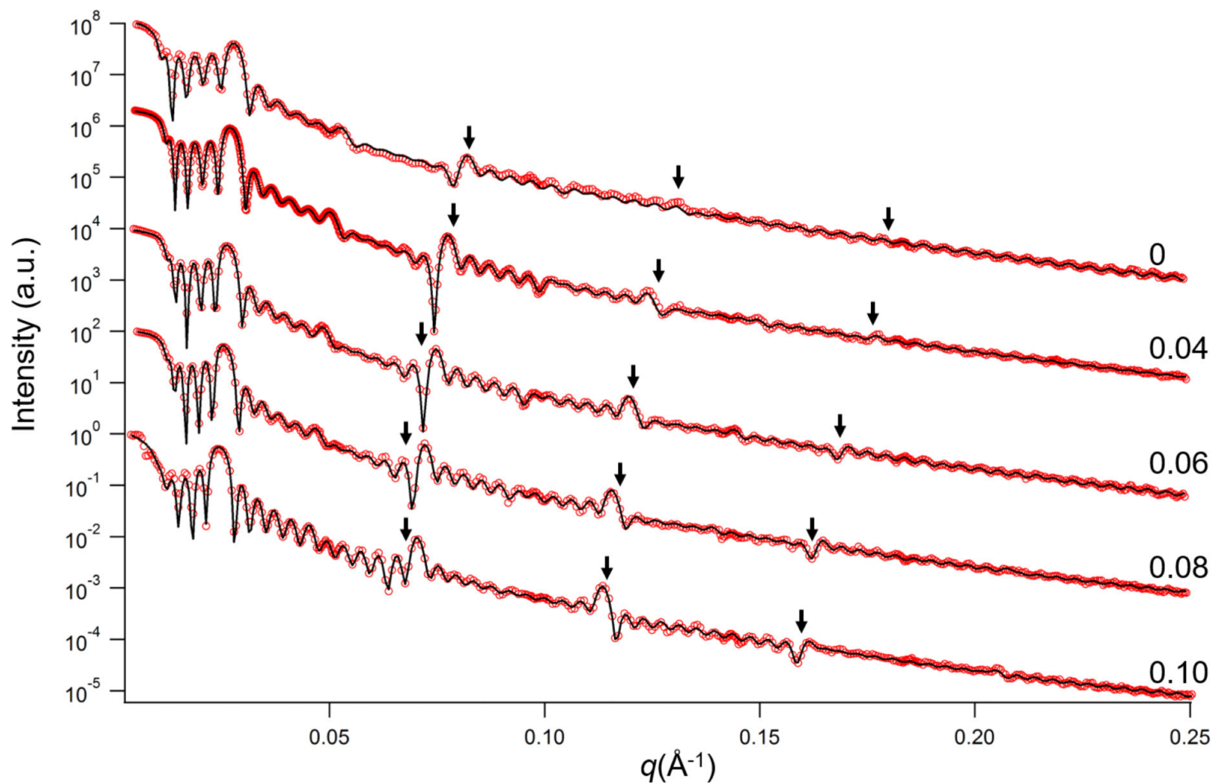

Figure 3:

RSoXR measurements conducted at 280 eV for PS-*b*-PMMA/[BMPR][TFSI] blends with ϕ_{IL} ranging from 0 – 0.10 (labeled on the right side). Experimental data is shown with red circles (○) and the simulated best fit shown in solid lines. The multilayer peak locations are indicated with arrows. Curves are vertically shifted arbitrarily for visual clarity.

NIST Author Manuscript

NIST Author Manuscript

NIST Author Manuscript

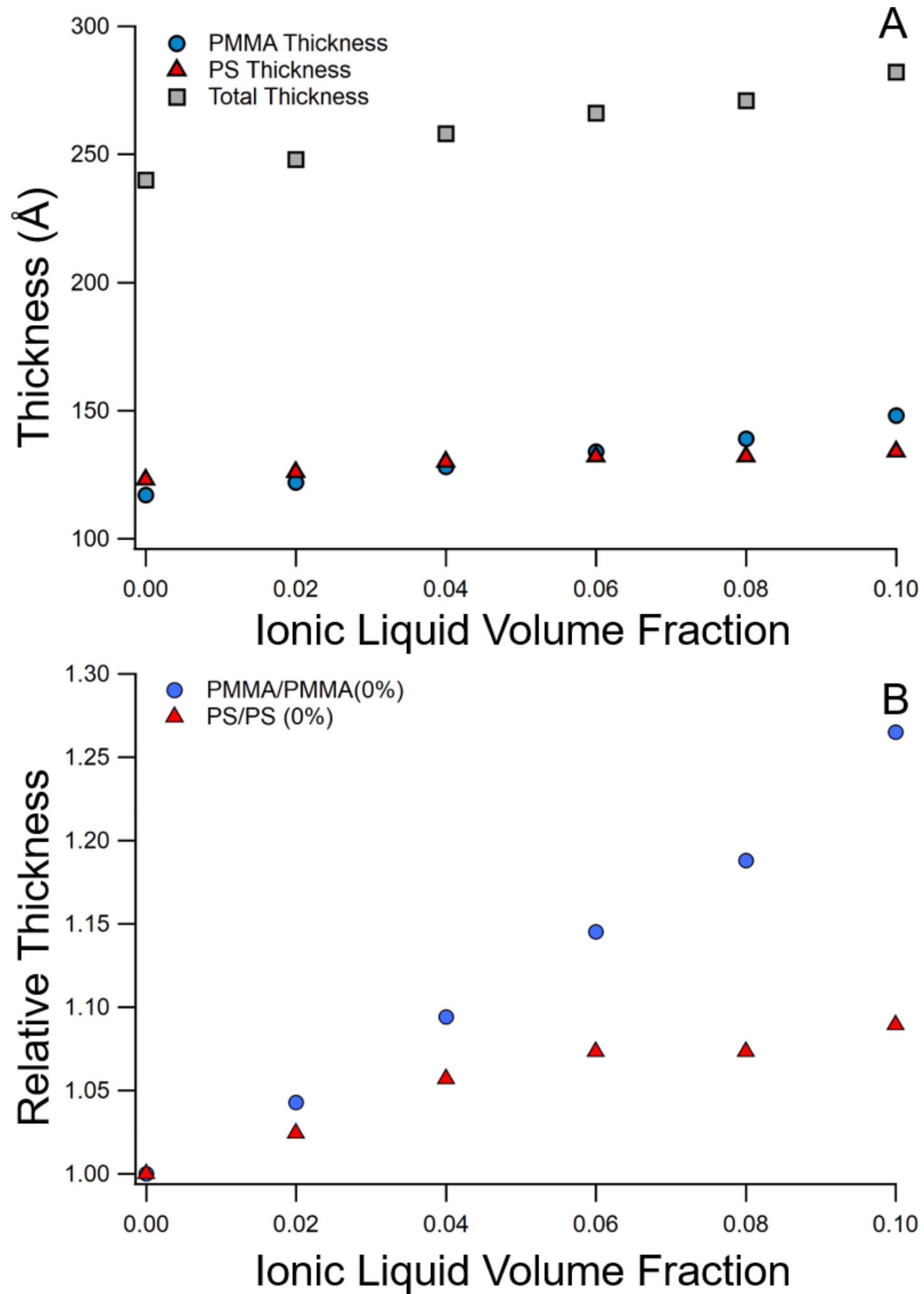

Figure 4:
Change in total period and thickness of individual layers as a function of of ϕ_{IL}. Changes are presented on both an absolute scale (A) and relative to the native BCP (B). Error bars are smaller than the symbols in all cases.

NIST Author Manuscript

NIST Author Manuscript

NIST Author Manuscript

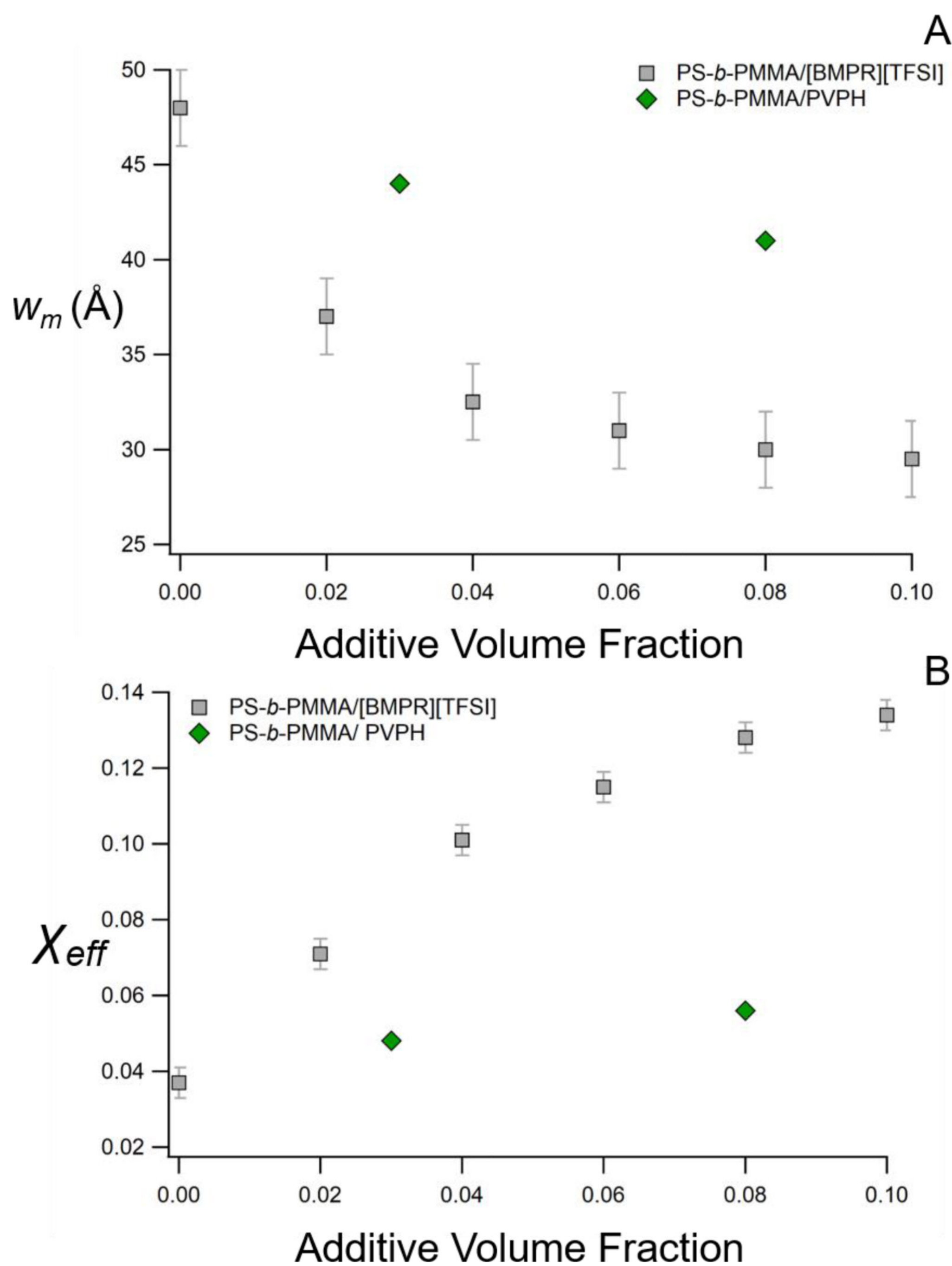

Figure 5:

Change in interface width (A) and χ_{eff} (B) as a function of ϕ_{IL}. Additionally literature data on blends of poly(vinyl phenol) (PVPH) with a similar PS-*b*-PMMA to the one used in this study is included for comparison (◆).[61]

NIST Author Manuscript

NIST Author Manuscript

NIST Author Manuscript

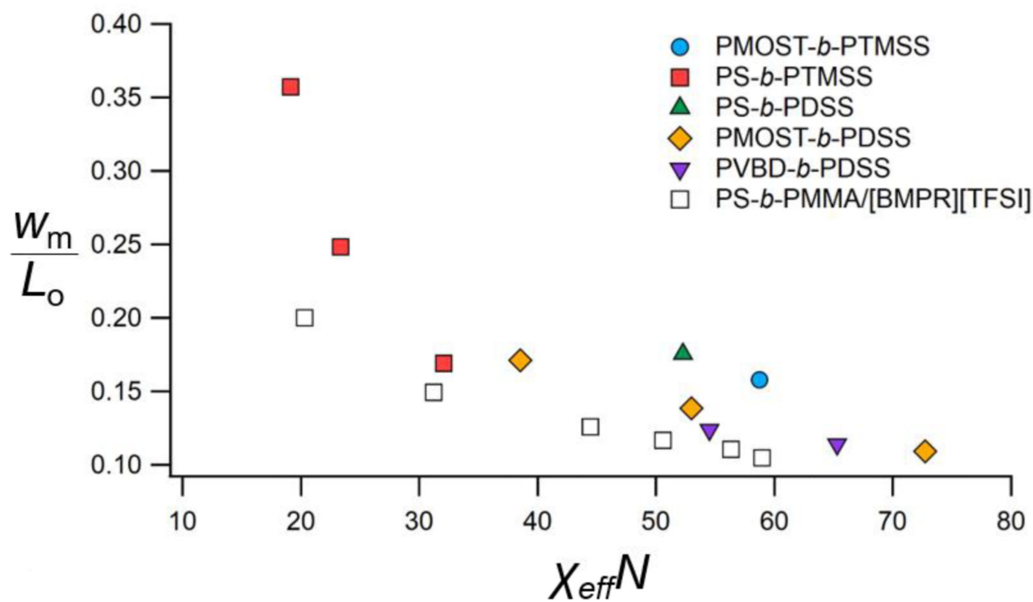

Figure 6:

w_m/L_0 as a function of $\chi_{eff}N$ for the IL/PS-*b*-PMMA blends, along with values from the literature for a series of BCPs, PS-*b*-poly(trimethylsilylstyrene) (PS-*b*-PTMSS), PS-*b*-PDSS, poly(4-methoxystyrene)-*b*-PDSS (PMOST-*b*-PDSS), PMOST-*b*-PTMSS and poly(5-vinyl-1,3-benzodioxole)-*b*-PDSS (PVBD-b-PDSS).[67]

NIST Author Manuscript

NIST Author Manuscript

NIST Author Manuscript

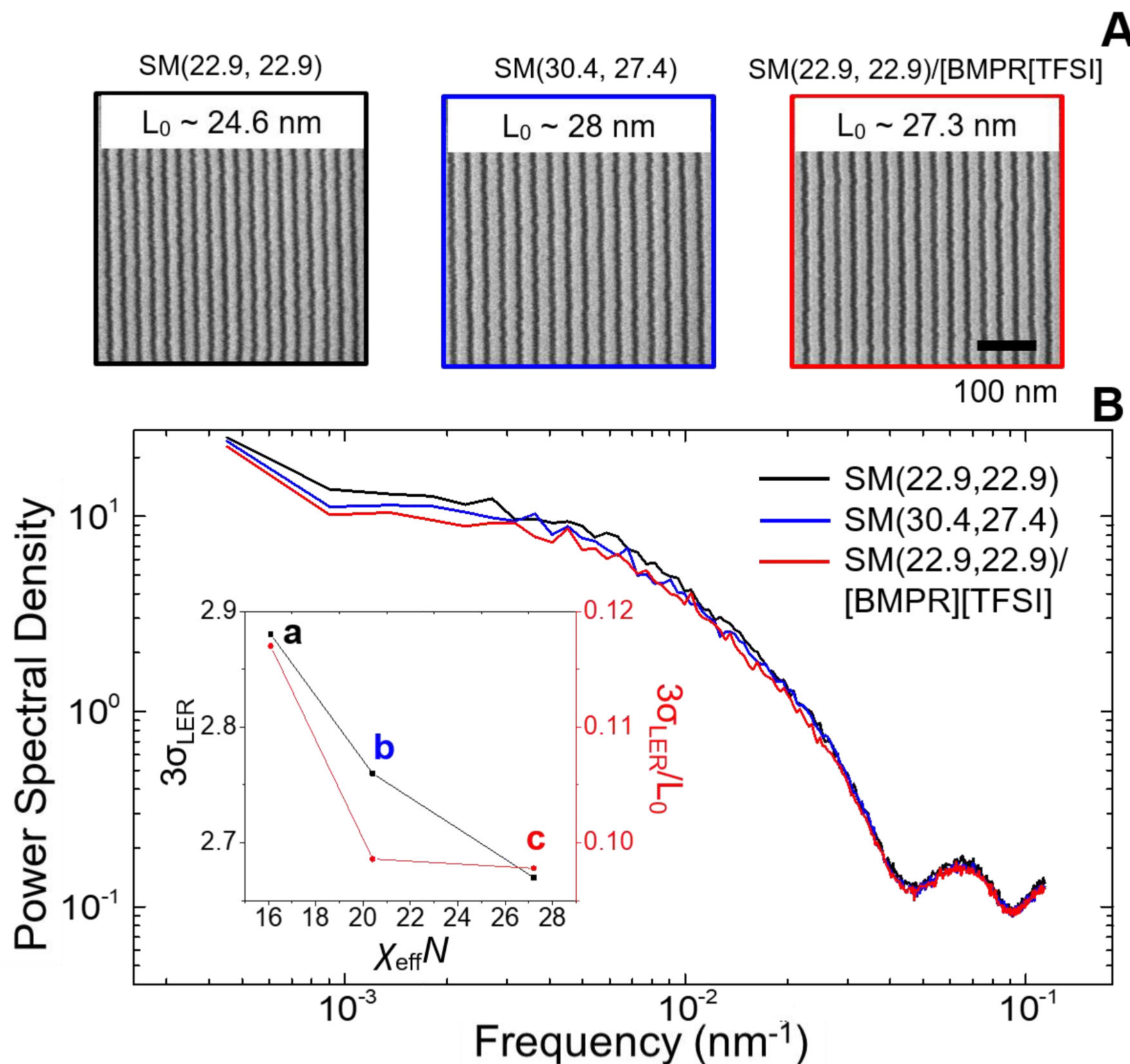

Figure 7.

A) Top-down SEM images in rectangular scan (0.45 um by 2.25 um area) of directed self-assembly of SM (22.9, 22.9), SM (30.4, 27.4) and SM (22.9, 22.9)/[BMPR][TFSI] (μ_{IL} = 0.08) blends; and B) corresponding PSD curves. The inset shows the $3\sigma_{LER}$ and normalized $3\sigma_{LER}$ (to L_0) as a function of the calculated $\chi_{eff}N$ value for the above three materials (a: SM (22.9, 22.9), b: SM (20.4,27.4), c: SM (22.9, 22.9)/[BMPR][TFSI]). 50 rectangular scans were analyzed for the PSD results. PMMA domains were removed for the measurements of line roughness.

Sample	Mn (PS) (kg/mol)	Mn (PMMA) (kg/mol)	f_{PS}	PDI	L_0 (nm)	Morphology
SM(22.9,22.9)	22.9	22.9	0.53	1.02	24.6	Lamellae
SM(30.4,27.4)	30.4	27.4	0.555	1.02	28	Lamellae
SM(39.5,37)	39.5	37	0.545	1.02	34.3	Lamellae

NIST Author Manuscript
NIST Author Manuscript
NIST Author Manuscript